8992 *Macromolecules* **2009**, *42*, 8992–8997
DOI: 10.1021/ma9011736

Macromolecules
ARTICLE

Spontaneous Appearance of Microdomains of Two Components at Poly(4-*tert*-butylstyrene-*block*-4-*tert*-butoxystyrene) Film Surfaces

Daisuke Kawaguchi, Hiroyuki Nomura, Siti Sarah Abdul Rahman, Minako Nakayama, and Yushu Matsushita*

Department of Applied Chemistry, Nagoya University, Furo-cho, Chikusa-ku, Nagoya 464-8603, Japan

Received May 31, 2009; Revised Manuscript Received September 2, 2009

ABSTRACT: We have prepared poly(4-*tert*-butylstyrene-*block*-4-*tert*-butoxystyrene), BO, having very bulky and hydrophobic substituent in both components by an anionic living polymerization. The BO films with various thicknesses were prepared by the spin-coating method from toluene solutions, and they were annealed under vacuum above the glass transition temperatures of both two components. An alternating lamellar structure oriented normal to the surface was observed at the surface of the BO film with thickness more than 150 nm, where the appearance of both B and O components were confirmed by XPS measurements. It is revealed that the ordered surface structure is caused by nanophase separation of BO clearly proved by hydrolyzed surface structures. Another aspect of this work is the structure of BO block copolymer after hydrolysis reaction. The O component can be easily converted into poly(4-hydroxystyrene) which has an ability to form a hydrogen bond. Moreover, it turns out that the control of the hydrolyzed layer thickness is possible by choosing the solvents in the reaction. This hydrophilic−hydrophobic nanopatterning is expected to be useful in a template of assembling nanoparticles and peptides.

1. Introduction

Nanophase-separated structures formed by self-assembled block copolymers have potential for applications of nanoporous materials,[1−6] template of nanoparticles,[7,8] catalytic surfaces, high conductivity nanocomposite,[9] and dye-sensitized solar cells,[10] etc. Orientation of microdomains in block copolymers is one of the most important subjects in block copolymer system for recent years. In general, one component in a diblock copolymer covers the surface due to minimizing the total free energy, and then, lamellar microdomains in a thin film tend to orient parallel to the surface and the substrate interface.[11−14] This phenomenon has been well-known as a surface-induced orientation. In order to utilize the nanophase-separated structures at the surface as well as in bulk to functional materials, external fields have been applied to block copolymer films. There have been many reports concerned with the orientation of the microdomains by external fields such as electric field,[15] magnetic field,[16,17] surface modification,[18−21] geometric substrate,[22] and solvent annealing,[23−25] etc. In this paper, we deal with spontaneous normal orientation of microdomains at a diblock copolymer surface.

We have investigated structures and chain orientation at surfaces of poly(4-trimethylsilylstyrene)/polyisoprene blend films by sum frequency generation and neutron reflectivity so far.[26] It was revealed that hydrophobic and bulky groups such as trimethylsilyl group are preferentially segregated at surfaces. On the basis of the result, it can be expected that very bulky hydrophobic substituent such as *tert*-butyl and *tert*-butoxy groups are preferentially enriched at surfaces as well as trimethylsilyl group. If there is a diblock copolymer having the bulky hydrophobic substituent in both components, the substituent is expected to emerge and to be segregated at the surface. In that case, the microdomains near the surface will spontaneously orient normal to the surface. Furthermore, the *tert*-butoxy group, which is one of the bulky hydrophobic substituents, can be easily converted to phenolic group by hydrolysis reaction. Hence, the combination of surface segregation and hydrolysis reaction of the *tert*-butoxy groups makes functional surfaces spontaneously. In this study, we show that surface structures of self-surface-directed block copolymer film and that of the subsequent hydrolyzed material.

2. Experimental Section

A polymer used in this study was poly(4-*tert*-butylstyrene-*block*-4-*tert*-butoxystyrene), which was abbreviated as BO. BO was synthesized by a sequential living anionic polymerization in THF at −78 °C under vacuum by using *sec*-butyllithium and isopropanol as an initiator and a terminator, respectively. Weight-averaged molecular weight, M_w, and molecular weight distribution, M_w/M_n, of BO were evaluated by light scattering and gel permeation chromatography, where M_n is a number-average molecular weight. The M_w and M_w/M_n of the sample were 658K and 1.08, respectively. Volume fraction of the O component in BO was estimated to be 0.46 based on ^{1}H NMR.

The surface free energies of B and O homopolymers were examined by contact angle measurement using a Dropmaster 300 (Kyowa Interface Science Co., Ltd.). Water and diiodemethane were used as probe liquids.

Morphology of the BO in bulk was evaluated by small-angle X-ray scattering (SAXS) measurement and transmission electron microscopy (TEM). The bulk BO sample was prepared by casting from 10% toluene solution. The thickness of the sample was ca. 0.5 mm. SAXS measurement was conducted using BL-15A at Photon Factory, High Energy Accelerator Research Organization, Japan. The wavelength of X-rays is 0.151 nm, and the camera length is 2.33 m. TEM observation was carried out using H-800 (Hitachi High Technologies) with acceleration voltage of 100 kV.

BO films were prepared by the spin-coating method from toluene solutions onto silicon wafers with native oxide layer. In order to reduce an effect of a surface free energy of a substrate on morphology, a BO film was prepared onto SiO_2-deposited polyimide film by the spin-coating method for cross-sectional

*To whom correspondence should be addressed: Fax +81-52-789-3210; Tel +81-52-789-4604; e-mail yushu@apchem.nagoya-u.ac.jp.

 Published on Web 10/28/2009

TEM observations. The films were dried under vacuum for at least 1 day and then annealed at 180 °C for at least 48 h in order to reach a stable state. Film thicknesses were determined on the basis of the height difference evaluated by atomic force microscopy (AFM) by scoring with a razor, and their values are approximately 150−470 nm. Surface structures of the films were characterized by intermittent contact mode AFM. AFM measurements were conducted by using an SPA 300HV with NanoNavi controller (Seiko Instruments Industry Co., Ltd.) at 293 K in air. A cantilever tip used for the observation was microfabricated from silicon, and its spring constant and resonant frequency were 2 N m^{-1} and 324 kHz, respectively. The interactions between an AFM cantilever tip and B, O, and H were evaluated by force−distance curve measurements. A cantilever tip used for the force curve measurements was microfabricated from Si_3N_4, and its spring constant was 0.42 N m^{-1}.

Surface morphologies of BO films were also investigated by field emission scanning electron microscopy, FE-SEM. FE-SEM observation was conducted using S-5200 (Hitachi High Technologies) with acceleration voltage of 3 kV. Cross-sectional TEM observation was carried out using JEM-1400EX (JEOL Ltd.) with acceleration voltage of 100 kV. For FE-SEM and TEM observations, the samples were stained by RuO_4 or OsO_4.

The composition of the BO film at the surface was examined by X-ray photoelectron spectroscopy (XPS). XPS measurements were conducted by using Phi ESCA 5800 X-ray photoelectron spectrometer (Physical Electronics Co. Ltd.). The X-ray source was Mg Kα X-ray operated at 14 kV and 30 mA. All C_{1s} peaks corresponding to neutral carbon were calibrated at the binding energy for 285.0 eV to correct for the charging energy shift. The analytical depth of XPS, d, from the outermost surface is given by

$$d = 3\lambda \sin\theta \quad (1)$$

where λ and θ are inelastic mean-free path and emission angle of photoelectrons, respectively.[27] According to Ashley's equation, λ for C_{1s} was estimated to be 3.1 nm,[28] while θ was varied from 15° to 90°.

The O component in BO films was hydrolyzed by an acid treatment into poly(4-hydroxystyrene), which is abbreviated as H. BO films were immersed into the mixture of water/HCl or methanol/HCl solution at 60 °C for 6 h. AFM observation was conducted to characterize the surface structures. To confirm the hydrolysis reaction, FT-IR measurements were carried out using FT/IR-6100 FT-IR spectrometer, JASCO International Co. Ltd. The samples for the IR measurements were prepared by Johnson method described as follows.[29] Some of the BO films after hydrolysis were covered with finely grounded KBr powder. The powder was rubbed on the surfaces using spatula with light pressure in order to attach the polymers to the powder surfaces. Although a large part of the BO films was scratched by the powder, the BO films still remained on the substrate. The KBr powder was pressed into the pellet. Hence, it is likely that the KBr sample includes a large fraction of the polymers existed near the film surfaces.

3. Results and Discussion

Total surface free energies of B and O, γ_B and γ_O, were evaluated by Owens' method.[30] The total surface free energy, γ, is expressed as the sum of two terms, i.e., γ^h and γ^d, where γ^h and γ^d denote the components of surface free energy due to hydrogen bonding and dispersion force, respectively. The γ_B and γ_O were 35.1 and 35.9 mJ m^{-2}, respectively, and they are much lower than that of polystyrene, γ_S, whose value is 40.7 mJ m^{-2}.[25] These results suggest that *tert*-butyl groups in B and *tert*-butoxy groups in O are highly oriented at the surfaces, lowering the surface free energy.

Structure of the BO in bulk was confirmed by TEM observation and SAXS measurements. Figure 1a shows a TEM image of BO. The sample was stained with OsO_4. The bright and dark regions denote B and O components, respectively. Figure 1b shows a SAXS profile of BO film. Integer peaks were weakly observed due to the less contrast of electron densities of B and O components. These results suggest that BO is in an ordered state and shows lamellar morphology. The average domain spacing estimated from the SAXS profile is ~76 nm.

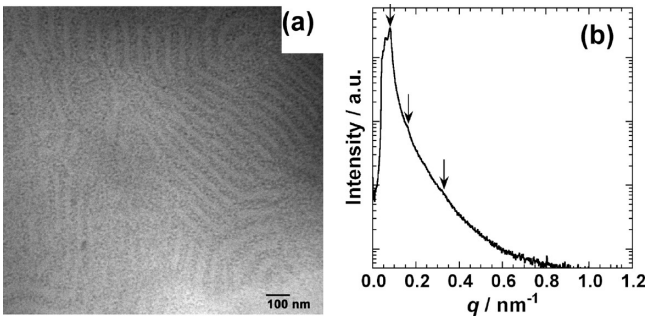

Figure 1. (a) TEM image and (b) SAXS profile of BO film. The dark part in (a) corresponds to O component selectively stained with OsO_4.

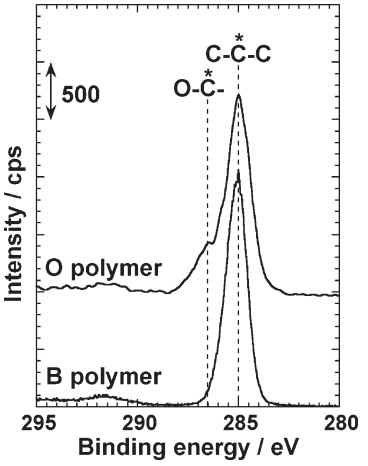

Figure 2. XPS C_{1s} core-level spectra of O and B homopolymers. Emission angle of photoelectron is 90°. The spectra were vertically shifted for clarity.

Surface Composition of BO Film. We tried to confirm the surface composition in BO film by the spectroscopic method. Before analyzing surface composition of BO film, XPS measurements for O and B homopolymers were carried out. Figure 2 shows XPS C_{1s} core-level spectra of O and B homopolymers. The C_{1s} spectrum of O homopolymer exhibits a main peak at 285.0 eV and a smaller one as a shoulder at 286.5 eV corresponding to neutral and ether carbons, respectively. The integral intensity of neutral carbon, I_{C-C}, and that of ether carbon, I_{C-O}, were evaluated based on a curve fit. The ratio of I_{C-O} to I_{C-C} in O homopolymer was 0.20. This value is in good agreement with the calculated value (= 0.20) from the chemical structure, that is, 2 ether carbons and 10 neutral carbons. On the other hand, the C_{1s} spectrum in B homopolymer shows a single peak at 285.0 eV. Hence, the fraction of O component at the BO film surface can be determined by the I_{C-O}/I_{C-C} value.

Figure 3 shows XPS C_{1s} core-level spectra of BO film as a function of emission angle of photoelectrons, θ. Tailing was observed near 286.5 eV for all the spectra in Figure 3, which reflects the existence of O component at the surface. The I_{C-C} and I_{C-O} values for the BO film were determined by a curve fit as the same way for O homopolymer. Figure 4a displays the sin θ dependence of I_{C-O}/I_{C-C} in the BO film. The I_{C-O}/I_{C-C} values are constant independent of sin θ.

In general, sin θ dependence of I_{C-O}/I_{C-C} does not reflect the volume fraction of O component in depth profile, ϕ_O, because photoelectrons mainly emitted from the region in close proximity to the surface. However, in this case, the I_{C-O}/I_{C-C} values are constant to be 8.3×10^{-2} irrespective of sin θ, meaning that surface segregation of one component does not occur within the range of analytical depth. The ϕ_O values can be calculated from eq 2.

$$\frac{I_{C-O}}{I_{C-C}} = \frac{2\phi_O}{10\phi_O + 12(1-\phi_O)} \quad (2)$$

Figure 4b shows sin θ dependence of ϕ_O in BO film. The solid line denotes the ϕ_O value in bulk evaluated by ^{1}H NMR.

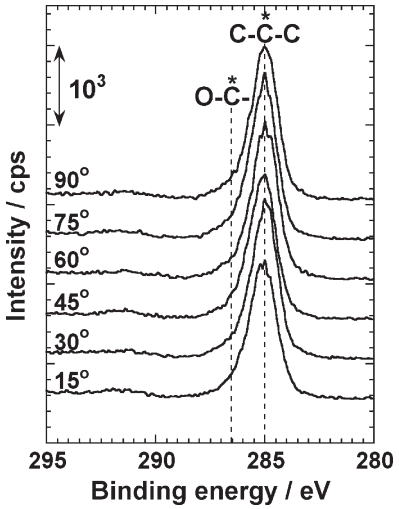

Figure 3. XPS C_{1s} core-level spectra of BO film as a function of emission angle of photoelectrons. The spectra were vertically shifted.

These results clearly tell us that both B and O components are bared at the BO block film surface as designed.

Morphology of BO Thin Film. Figure 5 shows AFM images for BO film before hydrolysis reaction, where the brighter region in Figure 5a corresponds to B component in BO. Ordered convex and concave structures are observed in Figure 5a. The average distance between the nearest convex is 74 nm, which is consistent with the domain spacing of BO evaluated by SAXS measurements. The height difference between high and low region is ~1 nm. This height difference may relate to the small difference in the surface free energies of the two components; however, the detail is unclear and needs further investigation. The corresponding phase image for BO film is shown in Figure 5b, the low contrast being observed. This is because both B and O components are in glassy state at room temperature, and there is no specific interaction between an AFM tip and B or O component.[31] Adhesion forces of B and O homopolymers being evaluated by force curve measurements are 6.9 ± 0.7 and 7.2 ± 1.0 nN, respectively.[31] On the basis of these results, it is most likely that both B and O components appear at the surface and the lamellar domains orient normal to the surface. These results were also observed in the samples with film thickness of more than 150 nm.

Figure 6a shows the top view of the FE-SEM image of BO film with thickness of 190 nm. The sample was stained with RuO_4 vapor. Since B component are more strongly stained by RuO_4 than O component, the brighter region in Figure 6a corresponds to B component. It is clearly seen that alternating lamellar domains orient normal to the surface near the surface of BO film. Figure 6b exhibits a cross-sectional TEM image of BO film supported by SiO_2-deposited polyimide film. In contrast to the FE-SEM image, the brighter region in the TEM image corresponds to the O component. No wetting layer was observed near the surface of BO film, and many of the microdomains near the surface oriented

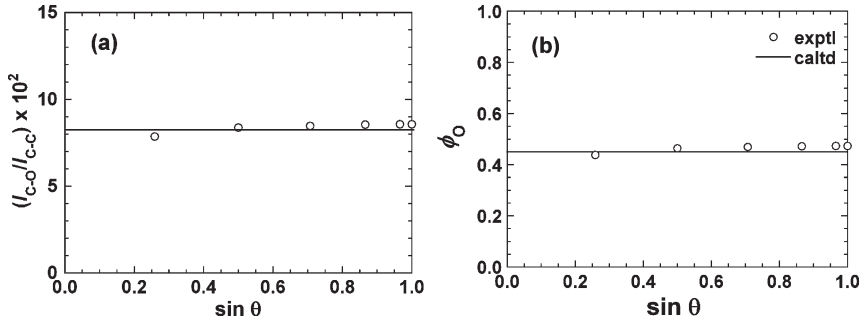

Figure 4. (a) Sin θ dependence of I_{C-O}/I_{C-C} values of BO film. Sin θ corresponds to the analytical depth. (b) Sin θ dependence of volume fraction of O component, ϕ_O, in BO film. The open circles are the experimental data calculated from eq 2. The solid line denotes the ϕ_O in bulk evaluated by ^{1}H NMR.

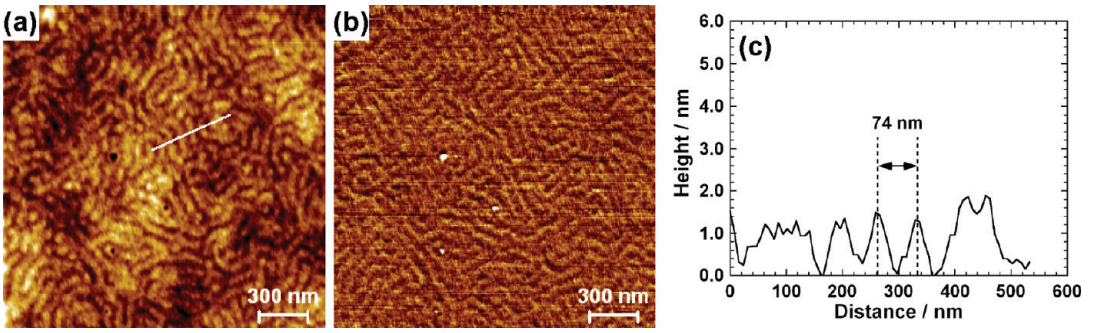

Figure 5. AFM images showing the nanophase-separated structure of BO with thickness of 200 nm. The bright part in the topography (a) and the slightly dark domain in the phase image (b) represent the B region. (c) Height profile along the line in (a). The distance between nearest convex is 74 nm on the average. Image size: 2 μm.

perpendicular to the surface whereas the microdomains near the substrate interface seem to orient parallel to the substrate. However, the alignment of microdomains through the film is not good as shown in Figure 6b. This may be due to the relatively small segregation power of B and O components.

Hydrolysis of BO Surface. To confirm the appearance of the two components at the surface and to fabricate a hydrophobic−hydrophilic nanopatterned surface, BO films were hydrolyzed by using an aqueous solution of hydrochloric acid. The ordered convex and concave structures were maintained or more evident even after hydrolysis as shown in Figure 7a. This means that the hydrolysis reaction does not affect the structure beneath the top surface as well as in the internal bulk. A contrast in a phase image was also clearly observed in Figure 7b. An adhesion force between a cantilever tip and H component was 9.5 ± 1.1 nN, which is higher than those for B and O components.[31] This means that a phase lag at H surface is larger than the others. Hence, it is reasonable to support that a brighter region in Figure 7b corresponds to the H component and a darker region corresponds to the B component in this experimental condition. The height difference after hydrolysis is ca. 3 nm, which is larger than the value before hydrolysis. One may think that the enhanced height difference is caused by an interaction between sample and cantilever tip. The force−distance curves for B, O, and H polymers shown in the Supporting Information are the typical ones for glassy polymers.[31] The slopes of the force curves in repulsive force region, which relate to moduli of the surfaces, are similar among the three components. The difference in the adhesion forces between H and B or H and O is not large. Hence, it is unlikely that the enhanced height difference of the hydrolyzed sample is caused by the change in the interaction with the cantilever tip. Furthermore, the total film thicknesses were measured by X-ray reflectivity measurements before and after hydrolysis, and they did not change. Since the B component cannot be hydrolyzed by water/HCl solution, this result seems reasonable. This result also indicates that the hydrolysis reaction locally occurs only at the surface. We speculate that the enhanced height difference by hydrolysis is caused by the shrinkage of H component at the surface, since the mass density of H is higher than that of O.

To confirm such a hypothesis, IR measurement was carried out. Figure 8 shows IR spectra of BO films before (broken line) and after (solid line) hydrolysis. A large peak appeared around 3400 cm^{-1} after hydrolysis which can be assigned as the O−H stretching mode. An aqueous solution of hydrochloric acid cannot penetrate into B, O, and H components because the solution is a nonsolvent for all three components. Hence, this result clearly indicates that the O component at the surface converted into H component through hydrolysis. The reason why the absorbance at 3400 cm^{-1} is large in comparison with that of C−H stretching around 2900 cm^{-1} is that the KBr sample was prepared by the Johnson method and included a large fraction of the polymers that existed near the film surfaces. Therefore, we could not quantitatively discuss the thickness of hydrolyzed layer of the film based on the IR results.

To verify the thickness of the hydrolyzed surface layer, XPS measurements were performed. In XPS measurements, only photoelectrons emitted from the region in close proximity to the surface can get out of the solid. The photoelectron intensity for j-core level at θ is expressed as

$$I_j(\theta) = Fk \int_0^\infty n_j(z) \exp\left\{\frac{-z}{\lambda_j \sin\theta}\right\} dz \qquad (3)$$

where z and $n_j(z)$ represent depth and atomic composition depth profile, respectively. F and k are the transmission function and a factor related to sensitivity. Hence, even though the sampling depth is z, photoelectrons are not

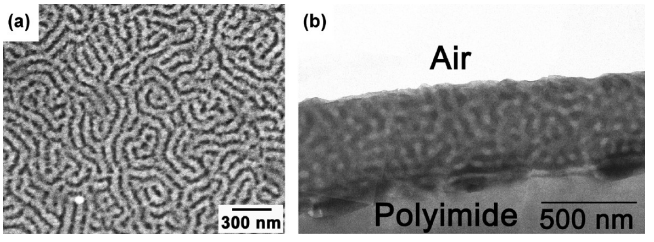

Figure 6. (a) FE-SEM image of BO film with thickness of 190 nm. (b) Cross-sectional TEM image of BO film supported by SiO_2-deposited polyimide film. Both samples were stained with RuO_4. The brighter region in FE-SEM and the darker region in TEM images correspond to B component.

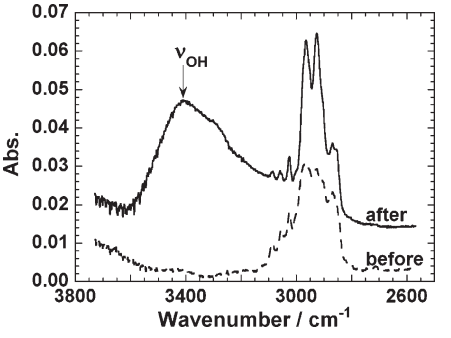

Figure 8. IR spectra of BO films before and after hydrolysis. The broken and solid lines denote before and after the reaction, respectively.

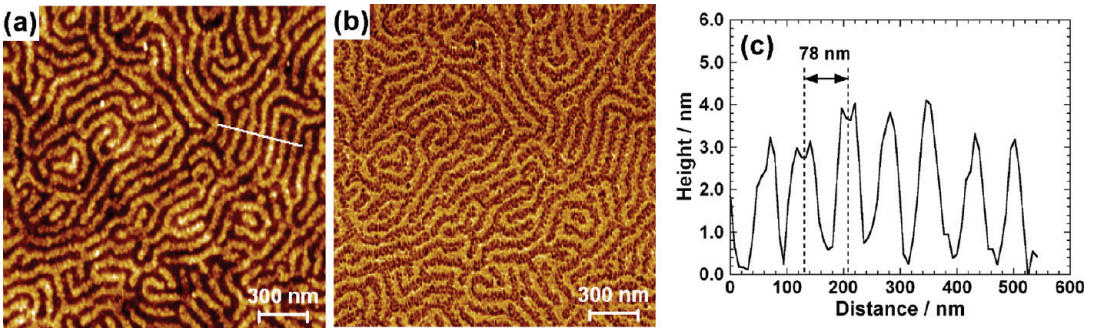

Figure 7. AFM images showing the nanophase-separated film of BO with thickness of 200 nm. The sample was hydrolyzed by using an aqueous solution of hydrochloric acid. The bright part in the topography (a) and the dark domain in the phase image (b) represent the B region. (c) Height profile along the line in (a). The average domain spacing is 78 nm, and height difference is 3 nm. Image size: 2 μm.

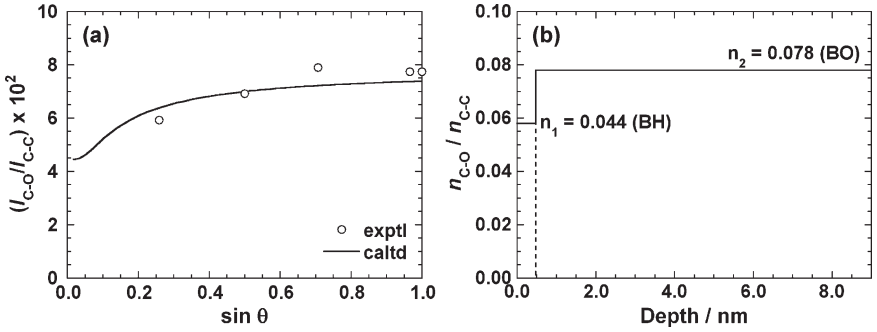

Figure 9. (a) Sin θ dependence of I_{C-O}/I_{C-C} in BO film after hydrolysis reaction using an aqueous solution of hydrochloric acid. The solid line in panel a represents the calculated value using eq 4 and model depth profile shown in panel b. (b) Model depth profile of the ratio of ether carbons to neutral carbons (n_{C-O}/n_{C-C}) assuming two layers; the hydrolyzed surface region (BH) and the nonhydrolyzed internal layer (BO).

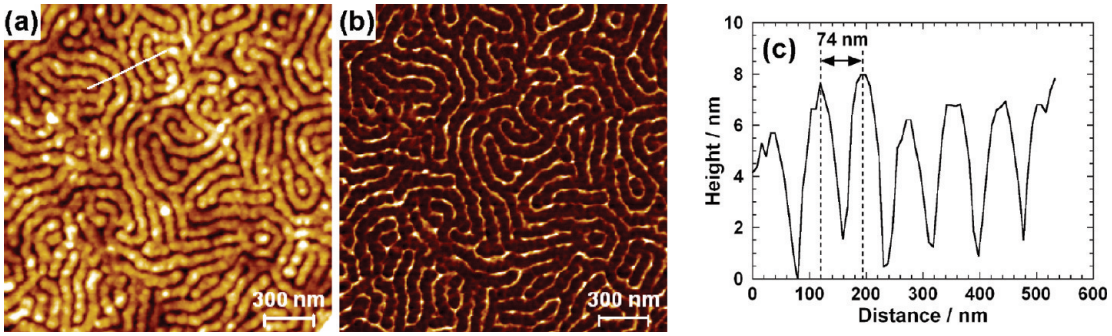

Figure 10. AFM images showing BO film after hydrolysis by using methanol solution of hydrochloric acid. (c) Height profile along the line in (a). Image size: 2 μm.

uniformly emitted from the depth region from the surface to z. Instead, the detected amount of photoelectrons exponentially decays with increasing depth. This means that the dependence of surface composition on sin θ cannot be simply regarded as the compositional depth profile. Thus, the following treatment was made to extract the real composition profile near the surface. On the basis of eq 3, the ratio of ether carbons to neutral carbons, (n_{C-O}/n_{C-C}), at a given θ can be expressed by

$$\frac{I_{C-O}}{I_{C-C}}(\theta) = \frac{\int_0^{z_1} n_{C-O} \exp\left\{\frac{-z}{\lambda_j \sin\theta}\right\} dz + \int_{z_1}^{z_2} n_{C-O} \exp\left\{\frac{-z}{\lambda_j \sin\theta}\right\} dz + \ldots}{\int_0^{z_1} n_{C-C} \exp\left\{\frac{-z}{\lambda_j \sin\theta}\right\} dz + \int_{z_1}^{z_2} n_{C-C} \exp\left\{\frac{-z}{\lambda_j \sin\theta}\right\} dz + \ldots} \quad (4)$$

Figure 9a shows sin θ dependence of I_{C-O}/I_{C-C} in BO film after hydrolysis. The I_{C-O}/I_{C-C} curve was calculated on the basis of eq 4. The open circles in Figure 9a are the experimental data, and the solid line denotes the fitted curve to the experimental data. We assume two layers in the model (n_{C-O}/n_{C-C}) profile. The top lalyer is the hydrolyzed surface region (BH), and the second one is the nonhydrolyzed internal layer (BO). The (n_{C-O}/n_{C-C}) values of BH and BO were calculated to be 4.4×10^{-2} and 7.8×10^{-2} based on the chemical structures and the bulk composition. The thickness of the top surface layer is only the fitting parameter. Figure 9b shows the model (n_{C-O}/n_{C-C}) profile for the best-fit curve in Figure 9a and should correspond to the real composition profile near the surface. The thickness of the surface layer hydrolyzed by acid is ca. 0.5 nm, indicating that the hydrolysis reaction occurs only at the surface of BO film when an aqueous solution of hydrochloric acid is used. On the basis of IR and XPS results, we can conclude that both B and O components in BO film appear at the surface and the lamellar domains orient normal to the surface and that the O domain at the surface can be almost completely hydrolyzed by acid.

Here it should be noted that these ordered structures were spontaneously appeared, whereas microdomains in the other block copolymer systems are oriented normal to the surface using external field such as electric or magnetic fields, confinement effect, substrate interaction, substrate roughness, etc. We speculate that the driving force of the normal orientation in our study is surface segregation of two side chain groups in polymer species adopted.

Effect of Solvents on Hydrolysis. When an aqueous solution of hydrochloric acid is used for hydrolysis reaction of BO film, the reaction takes place only at the surface. If a methanol solution of hydrochloric acid is used, it is expected that the reaction occurs through the film because H component which is produced after the reaction can be soluble in methanol. Figure 10 shows topographic and phase images of BO film after hydrolysis reaction using a methanol solution of hydrochloric acid. After the hydrolysis reaction, the sample was just rinsed with water and not dried before AFM observation. Comparing Figure 10 with Figure 7, the ordered convex and concave structure is still observed, and the domain spacing is maintained to be 74 nm; however, the width at the higher part in the topographic image became larger. The height difference of the structure is ca. 6 nm, which is much larger than that formed by the hydrolysis using an aqueous solution of hydrochloric acid. The higher part in the topographic image corresponds to the darker region in the phase image. This means that H chain should be swollen by the methanol solution of hydrochloric acid.

This phenomenon cannot be observed solely due to the small difference in γ. It is known that the surface free energies of polystyrene and poly(methyl methacrylate) are quite small and their values are 40.7 and 41.1 mJ m^{-2}, respectively.[32] Nevertheless, polystyrene component tends to be segregated at the surface of the block copolymer thin film. Russell and co-workers reported that poly(styrene-*block*-methyl methacrylate) diblock copolymer in thin film forms lamellar structure parallel to the surface and polystyrene component covers the surface in a quasi-equilibrium state.[10] Hence, the very small difference in γ is not the necessary and sufficient condition to obtain the self-surface oriented copolymer film. In contrast, lamellar domains near the BO surface orient normal to the surface although there is a small difference between γ_B and γ_O. Hence, we propose that the orientation of side-chain groups in copolymers is one of the important factors to control the orientation of microdomains.

4. Conclusions

We have prepared poly(4-*tert*-butylstyrene-*block*-4-*tert*-butoxystyrene), BO, having very bulky and hydrophobic substituent in both components by an anionic living polymerization. The lamellar domains oriented normal to the surface were observed at the surface of the BO film with thickness more than 150 nm. The appearance of both B and O components was confirmed by XPS measurements. It is proved that the surface ordered structure is caused by nanophase separation of BO clearly proved by the hydrolyzed surfaces.

Another aspect of this work deals with the structure of BO block copolymer after hydrolysis reaction. The O component can be easily converted into poly(4-hydroxystyrene). It is possible to control the thickness of the hydrolyzed layer by choosing the solvents in the reaction. This hydrophilic−hydrophobic nanopatterning which has hydrogen-bonding site is expected to be useful in a template of assembling nanoparticles and peptides.

Acknowledgment. This research was in part supported by the Grant-in-Aids for Young Scientists B (No. 17750108) and for the Priority Area "Soft Matter Physics" (No. 863) for the Global COE program "Elucidation and Design of Materials and Molecular Functions" from the Ministry of Education, Culture, Sports, Science and Technology (MEXT), Japan. This wok was also supported by Nanotechnology Network Project (Kyushu-area Nanotechnology Network) of MEXT, Japan. This work was performed using BL-15A of Photon Factory, Institute of Materials Structure Science, High Energy Accelerator Research Organization, Japan. The authors acknowledge the Division for Medical Research Engineering, Nagoya University Graduate School of Medicine, for technical support of TEM observations. SEM observations were conducted at Venture Business Laboratory, Nagoya University. D.K. thanks the Hattori Houkokai for financial support.

Supporting Information Available: Experimental details of AFM observation and force curve measurements. This material is available free of charge via the Internet at http://pubs.acs.org.

References and Notes

(1) Chan, V. Z. H.; Hoffman, J.; Lee, V. Y.; Iatrou, H.; Avgeropoulos, A.; Hadjichristidis, N.; Miller, R. D.; Thomas, E. L. *Science* **1999**, *286*, 1716–1719.
(2) (a) Mao, H.; Hillmyer, M. A. *Macromolecules* **2005**, *38*, 4038–4039. (b) Kubo, T.; Wang, R. F.; Olson, D. A.; Rodwogin, M.; Hillmyer, M. A.; Leighton, C. *Appl. Phys. Lett.* **2008**, *93*, 13112.
(3) (a) Li, L.; Yokoyama, H.; Sugiyama, K.; Nemoto, T. *Adv. Mater.* **2004**, *16*, 1226–1229. (b) Lei, L.; Yokoyama, H.; Nemoto, T.; Sugiyama, K. *Adv. Mater.* **2004**, *16*, 1542–1546.
(4) Uehara, H.; Yoshida, T.; Kakiage, M.; Yamanobe, T.; Komoto, T.; Nomura, K.; Nakajima, K.; Matsuda, M. *Macromolecules* **2006**, *39*, 3971–3974.
(5) Kamperman, M.; Garcia, C. B. W.; Du, P.; Ow, H. S.; Wiesner, U. *J. Am. Chem. Soc.* **2004**, *126*, 14708–14709.
(6) (a) Komura, M.; Iyoda, T. *Macromolecules* **2007**, *40*, 4106–4108. (b) Watanabe, R.; Kamata, K.; Iyoda, T. *J. Mater. Chem.* **2008**, *18*, 5482–5491.
(7) Balazs, A. C.; Emrick, T.; Russell, T. P. *Science* **2006**, *314*, 1107–1110.
(8) Lin, Y.; Boker, A.; He, J.; Sill, K.; Xiang, H.; Abetz, C.; Li, X.; Wang, J.; Emrick, T.; Long, S.; Wang, Q.; Balazs, A. C.; Russell, T. P. *Nature* **2005**, *434*, 55–59.
(9) Cho, B. K.; Jain, A.; Gruner, S. M.; Wiesner, U. *Science* **2004**, *305*, 1598–1601.
(10) Watkins, P. K.; Walker, A. B.; Verschoor, G. L. B. *Nano Lett.* **2005**, *5*, 1814–1818.
(11) (a) Anastasiadis, S. H.; Russell, T. P.; Satija, S. K.; Majkrazak, C. F. *Phys. Rev. Lett.* **1989**, *62*, 1852–1855. (b) Anastasiadis, S. H.; Russell, T. P.; Satija, S. K.; Majkrazak, C. F. *J. Chem. Phys.* **1990**, *92*, 5677–5691. (c) Russell, T. P.; Coulon, G.; Deline, V. R.; Miller, D. C. *Macromolecules* **1989**, *22*, 4600–4606.
(12) Torikai, N.; Noda, I.; Karim, A.; Satija, S. K.; Han, C. C.; Matsushita, Y.; Kawakatsu, T. *Macromolecules* **1997**, *30*, 2907–2914.
(13) Matsen, M. W. *Macromolecules* **2006**, *39*, 5512–5520.
(14) Yokoyama, H.; Mates, T. E.; Kramer, E. J. *Macromolecules* **2000**, *33*, 1888–1898.
(15) (a) Morkved, T. L.; Lu, M.; Urbas, A. M.; Ehrichs, E. E.; Jaeger, H. M.; Mansky, P.; Russell, T. P. *Science* **1996**, *273*, 931–933. (b) Ashok, B.; Muthukumar, M.; Russell, T. P. *J. Chem. Phys.* **2001**, *115*, 1559–1564. (c) Thurn-Albrecht, T.; Derouchey, J.; Russell, T. P.; Jaeger, H. M. *Macromolecules* **2000**, *33*, 3250–3253. (d) Thurn-Albrecht, T.; Derouchey, J.; Russell, T. P.; Kolb, R. *Macromolecules* **2002**, *35*, 8106–8110. (e) Xu, T.; Zvelindovsky, A. V.; Sevink, G. J. A.; Lyakhova, K. S.; Jinnai, H.; Russell, T. P. *Macromolecules* **2005**, *38*, 10788–10798.
(16) Osuji, C.; Ferreira, P. J.; Mao, G.; Ober, C. K.; Sande, J. B. V.; Thomas, E. L. *Macromolecules* **2004**, *37*, 9903–9908.
(17) Tomikawa, N.; Lu, Z. B.; Itoh, T.; Imrie, C. T.; Adachi, M.; Tokita, M.; Watanabe, J. *Jpn. J. Appl. Phys., Part 2* **2005**, *44*, L711–L714.
(18) (a) Yang, X. M.; Peters, R. D.; Nealey, P. F.; Solak, H. H.; Cerrina, F. *Macromolecules* **2000**, *33*, 9575–9582. (b) Kim, S. O.; Solak, H. H.; Stoykovich, M. P.; Ferrier, N. J.; de Pablo, J. J.; Nealey, P. F. *Nature* **2003**, *424*, 411–414. (c) Stoykovich, M. P.; Muller, M.; Kim, S. O.; Solak, H. H.; Edwards, E. W.; de Pablo, J. J.; Nealey, P. F. *Science* **2005**, *308*, 1442–1446.
(19) (a) In, I.; La, Y.-H.; Park, S. M.; Nealey, P. F.; Gopalan, P. *Langmuir* **2006**, *22*, 7855–7860. (b) Han, E.; In, I.; Park, S. M.; La, Y.-H.; Wang, Y.; Nealey, P. F.; Goplan, P. *Adv. Mater.* **2007**, *19*, 4448–4452. (c) Han, E.; Sruen, K. O.; La, Y.-H.; Nealey, P. F.; Gopalan, P. *Macromolecules* **2008**, *41*, 9090–9097.
(20) Tada, Y.; Akasaka, S.; Yoshida, H.; Hasegawa, H.; Dobisz, E.; Kercher, D.; Takenaka, M. *Macromolecules* **2008**, *41*, 9267–9276.
(21) (a) Ryu, D. Y.; Shin, K.; Drockernmuller, E.; Hawker, C. J.; Russell, T. P. *Science* **2005**, *308*, 236–239. (b) Ham, S.; Shin, C.; Kim, E.; Ryu, D. Y.; Jeong, U.; Russell, T. P.; Hawker, C. J. *Macromolecules* **2008**, *41*, 6431–6437.
(22) Segalman, R. A.; Yokoyama, H.; Kramer, E. J. *Adv. Mater.* **2001**, *13*, 1152–1155.
(23) Kim, S. H.; Misner, M. J.; Xu, T.; Kimura, M.; Russell, T. P. *Adv. Mater.* **2004**, *16*, 226–231.
(24) Xuan, Y.; Peng, J.; Cui, L.; Wang, H.; Li, B.; Han, Y. *Macromolecules* **2004**, *37*, 7301–7307.
(25) Sakurai, S.; Bando, H.; Yoshida, H.; Fukuoka, R.; Mouri, M.; Yamamoto, K.; Okamoto, S. *Macromolecules* **2009**, *42*, 2115–2121.
(26) (a) Kawaguchi, D.; Ohya, M.; Torikai, N.; Takano, A.; Matsuhita, Y. *Polym. J.* **2007**, *39*, 1274–1280. (b) Kawaguchi, D.; Zhang, L.; Ouchi, Y.; Ohya, M.; Takano, A.; Matsushita, Y. Manuscript in preparation.
(27) Andrade, J. D. *Surface and Interfacial Aspects of Biomedical Polymers. Surface Chemistry and Physics*; Plenum: New York, 1985.
(28) Ashley, J. C. *IEEE Trans. Nucl. Sci.* **1980**, *NS-27*, 1454.
(29) Nishikida, K.; Nishio, E.; Hannah, R. W. *Selected Applications of Modern FT-IR Techniques*; Kodansha Ltd.: Tokyo, Japan, 1995.
(30) Owens, D. K.; Wendt, R. C. *J. Appl. Polym. Sci.* **1969**, *13*, 1741–1747.
(31) We compared contrast in phase images with adhesion forces in the B, O, and H polymer system. See Supporting Information.
(32) Wu, S. In *Polymer Handbook*, 4th ed.; Brandrup, J., Immergut, E. H., Gruke, E. A., Eds.; Wiley-Interscience: New York, 1999; p VI-525.